

Defect-Mediated Polarization Switching in Ferroelectrics and Related Materials: From Mesoscopic Mechanisms to Atomistic Control

By Sergei V. Kalinin,* Brian J. Rodriguez,* Albina Y. Borisevich,* Arthur P. Baddorf, Nina Balke, Hye Jung Chang, Long-Qing Chen, Samrat Choudhury, Stephen Jesse, Peter Maksymovych, Maxim P. Nikiforov, and Stephen J. Pennycook

The plethora of lattice and electronic behaviors in ferroelectric and multi-ferroic materials and heterostructures opens vistas into novel physical phenomena including magnetoelectric coupling and ferroelectric tunneling. The development of new classes of electronic, energy-storage, and information-technology devices depends critically on understanding and controlling field-induced polarization switching. Polarization reversal is controlled by defects that determine activation energy, critical switching bias, and the selection between thermodynamically equivalent polarization states in multiaxial ferroelectrics. Understanding and controlling defect functionality in ferroelectric materials is as critical to the future of oxide electronics and solid-state electrochemistry as defects in semiconductors are for semiconductor electronics. Here, recent advances in understanding the defect-mediated switching mechanisms, enabled by recent advances in electron and scanning probe microscopy, are discussed. The synergy between local probes and structural methods offers a pathway to decipher deterministic polarization switching mechanisms on the level of a single atomically defined defect.

and the introduction of novel information storage and computational mechanisms, necessitates the development of a new generation of devices utilizing lattice, spin, and orbital degrees of freedom.^[1] Transition metal oxides have long been viewed as uniquely suited for this purpose, giving rise to the concept of oxide electronics. Among functional oxides, ferroelectric and antiferroelectric materials have emerged as primary functional building blocks due to the ability of these materials to undergo fast reversible bias-induced phase transitions and, thus, to effectively store information (ferroelectrics) or energy (antiferroelectrics). In addition, strong coupling between polarization, strain, and electronic properties at surfaces and interfaces enables a broad spectrum of magnetoelectronic and strain-coupled devices.

1. Introduction

The evolution of information and electronic materials technologies, including shrinking device size, increasing operation speed,

1.1. What Makes a Ferroelectric Material?

The crystallographic structure of a prototypical ferroelectric perovskite, BaTiO₃ (BTO), is illustrated in Figure 1a. The Ba and O atoms form a rigid framework, with Ti cations residing in octahedral sites. At high temperatures, each Ti atom is at the center of an oxygen octahedron, and the structure of the material is cubic. Below the Curie temperature (e.g., 400 K for BTO), the central cation (Ti) shifts along one of six (100) directions, resulting in a dipole and an associated cubic-to-tetragonal phase transition, and accompanying lattice deformation. The orientation of the dipole can be manipulated by an external electric field (polarization switching (Fig. 1b)), which gives rise to the many applications based on ferroelectric materials.^[2]

Critical for understanding ferroelectrics is the fact that dipoles in adjacent cells are strongly coupled, giving rise to an order parameter field describing collective atomic displacements.^[3] Many phenomena in ferroelectrics can be described on the mesoscopic scale as the evolution of the order parameter field described by the Ginzburg–Landau–Devonshire theory.^[2] The role of atomistic effects at surfaces, interfaces, and defects is introduced through appropriate boundary conditions and built-in

[*] Dr. S. V. Kalinin, Dr. S. J. Pennycook, Dr. A. Y. Borisevich, Dr. A. P. Baddorf, Dr. N. Balke, Dr. H. J. Chang, Dr. S. Jesse, Dr. P. Maksymovych, Dr. M. P. Nikiforov
Oak Ridge National Laboratory
Oak Ridge, TN 37831 (USA)
E-mail: sergei2@ornl.gov; albinab@ornl.gov
Dr. B. J. Rodriguez
Conway Institute of Biomolecular and Biomedical Research
University College Dublin
Belfield, Dublin 4 (Ireland)
E-mail: brian.rodriguez@ucd.ie
Prof. L.-Q. Chen, Dr. S. Choudhury
Department of Materials Science and Engineering
Pennsylvania State University
University Park, PA 16802 (USA)

DOI: 10.1002/adma.200900813



Dr. Sergei V. Kalinin is currently a research staff member at the Oak Ridge National Laboratory (Ph.D. 2002 University of Pennsylvania). His current research interests include nanoscale physics of ferroelectric and multiferroic oxides, coupling between electromechanical, electrical, and transport phenomena, and electrostatic and

electromechanical interactions in liquids, biosystems, and molecular systems.



Dr. Brian J. Rodriguez is currently a Lecturer in Nanoscience at the Conway Institute of Biomolecular and Biomedical Research at University College Dublin. He completed his Ph.D. in Physics at North Carolina State University in 2003 and subsequently held postdoctoral appointments at North Carolina State University and at Oak Ridge National Laboratory. In

2007, he received an Alexander von Humboldt fellowship and carried out his research at the Max Planck Institute of Microstructure Physics in Halle, Germany.



Dr. Albina Y. Borisevich is currently a research staff member at the Oak Ridge National Laboratory (Ph.D. 2002 University of Pennsylvania). She is working in the field of aberration-corrected transmission electron microscopy. Her specific research interests include high-resolution imaging and spectroscopy of ferroelectric oxides, in situ electrical

measurements in TEM, combined scanning probe and TEM modes, and structure–property relations in heterogeneous catalysts.

effective fields, while the role of the underpinning lattice is approximated by the periodic Peierls potential.^[4]

Crucial for device applications of ferroelectric materials is the polarization behavior at surfaces and interfaces (broken symmetry). A polarization discontinuity results in a charge density, associated with high electrostatic depolarization energy that suppresses the stability of the ferroelectric phase for small sizes. The depolarization energy is minimized through screening processes that include the formation of antiparallel domain structures, adsorption of charged species on the surfaces, or

surface chemical reactions. At the same time, polarization-induced changes in the electronic structure provide a degree of freedom in device design.

Note that the physics of the screening phenomena represents the most drastic difference between ferroelectric and ferromagnetic materials. The smaller width of the domain wall in ferroelectrics (1–2 nm, as compared with 10–100 nm in ferromagnets) enables higher storage densities but at the same time results in much higher wall and depolarization energies. Due to the lack of elementary magnetic charges, long-range magnetic force interactions are less sensitive to the structure and surface states of the material. At the same time, ferroelectric devices based on the ferroelectric field effect are strongly dependent on surface and interface properties, where the presence of free charge (atmosphere for data storage, mobile ions, oxygen vacancies, and interface states for heterostructures) will effectively screen ferroelectric polarization. This necessitates much more stringent requirements for materials and device fabrication and opens pathways for interface-controlled devices. This situation is conceptually similar to ferromagnetic tunneling devices and spintronic devices, the properties of which are also controlled by interfaces.

1.2. Ferroelectrics in Information Technologies

Polarization switching in ferroelectric materials has been proposed as a functional basis for non-volatile memory devices and information technology since the 1950s. The simplicity of the concept – using an electric field to manipulate the ferroelectric polarization with an appropriate readout for data recovery – has long been belied by the difficulty of experimental implementation, primarily due to roadblocks in materials synthesis and device integration.

Initial progress in the field was achieved in the mid-1990s, when the development of film-growth technologies and the refinement of sol–gel synthesis allowed mass production of polycrystalline ferroelectric films and their integration with noble and base metal electrodes.^[5] This opened a pathway for the mass production of ferroelectric dynamic random access memory (DRAM)-type devices, in which the oxide in the capacitor is substituted by a ferroelectric material, providing the advantage of non-volatility (e.g., Fig. 1c). This, in turn, allows for reduced power consumption, stability with respect to power loss, and radiation hardening. Note that in modern semiconductor technologies, the preference for dual- and quadruple-core processors over increased computational power of a single processor is a direct consequence of limits in power management. Currently, commercial ferroelectric RAM (FeRAM) devices are available from Fujitsu, Toshiba, and Ramtron, and are broadly used in cell phones, smart cards, automotive applications, and some video-game consoles (e.g., Sony PlayStation 2).

In the late 1990s, the concept of ferroelectric-based data storage emerged (Fig. 1d).^[6] Ferroelectric bits are written on a continuous or nanopatterned substrate, similar to magnetic bits in conventional hard drives. The significant advantages of ferroelectric data storage are a) the extremely thin (1–2 unit cells) domain walls, potentially allowing molecular-scale (100–1000 TBit in⁻²) storage density, and b) the simplicity of the electric writing process. As a harbinger of future developments, ~8-nm bit size, corresponding to ~10 TByte in⁻² storage density, has been demonstrated

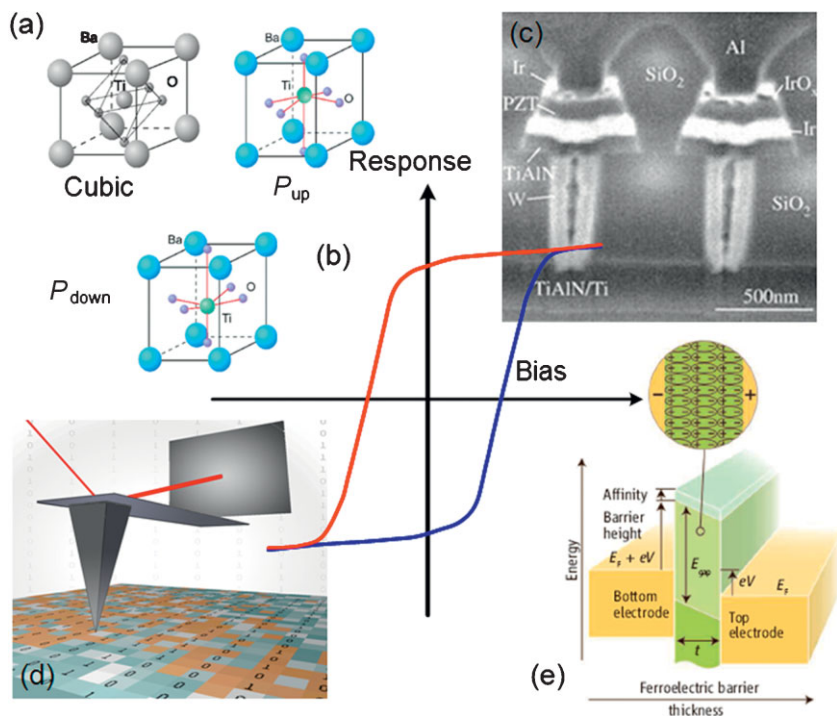


Figure 1. a) The crystal structure of cubic barium titanate and the tetragonal distortion of the unit cell for “up” and “down” polarization states. b) Ferroelectric hysteresis loop demonstrates the switchable polarization between the “up” and “down” polarization states in (a). c) Schematic image of a non-volatile ferroelectric random access memory device. d) Depiction of ferroelectric data storage. e) Schematic image of a ferroelectric tunneling barrier. Panels (a) and (e) reprinted with permission from [46] and [47]. Copyright 2004 and 2006, respectively, American Association for the Advancement of Science. Panel (c) reproduced with permission from [48]. Copyright 2001, American Institute of Physics. Panel (d) reproduced from [49].

experimentally and the recent demonstration of ~ 2 -nm isolated domains (~ 160 TByte in $^{-2}$) suggests that this is not the limit.^[7] Finally, the recent discovery of polarization-dependent resistivity in perovskite tunneling barriers (Fig. 1e),^[8] following earlier work in ferroelectric polymers,^[9] suggests enormous potential in information technology, including resistive memory architectures and direct electroresistive recording.^[10]

The examples above illustrate the role ferroelectrics play in information technology, ranging from well-established and commercialized fields to emerging applications. The coupling between ferroelectric, ferroelastic, and ferromagnetic order parameters in multiaxial and improper ferroelectrics and multiferroics opens additional pathways for electronic applications, for example, magnetic-field sensors and readout heads. Further scaling of FeRAMs to the nanoscale, as well as novel storage and tunneling applications, require understanding of the structural mechanisms of polarization switching, as well as the role of defects and interfaces on this process.

1.3. Defects in Ferroelectric Materials

The often governing role of defects on materials functionality is one of the underpinnings of materials science and condensed-

matter physics, with multiple examples from the field of structural materials, semiconductors, and superconductors. The rapid progress in semiconductor technology has been enabled by advances in materials fabrication as well as progress in understanding the atomic and electronic structure of defects. In comparison, the role of defects in ferroelectrics is significantly more complicated. The typical perovskite lattice allows for a broad range of point (particularly oxygen vacancies) and extended defects that affect polarization stability and also create space charge and strain fields in the material. Unlike electrostatic interactions in semiconductors that are typically screened on the scale of the corresponding Debye length (≈ 10 – 100 nm), the screening lengths in ferroelectrics are generally much larger. In many cases, the electrostatic and particularly the elastic fields in the material will be non-local and determined by the boundary conditions, precluding simple descriptions of device functionality.

For ferroelectric device applications, the role of defects on polarization dynamics is especially relevant. In ferroelectric materials, defects control the local polarization stability, act as pinning sites for domain-wall motion,^[11,12] and nucleation sites for polarization reversal. In particular, defects can control the kinetic pathways for polarization switching in thermodynamically equivalent states, for example, in (100)-oriented rhombohedral ferroelectrics. However, to date, experimental studies relating defect structures to pinning and nucleation have invariably been limited by two major factors: a) only the collective effect of multiple defects of different types on an average system response were probed, and b) the type of defects and polarization switching mechanisms on a single-defect level were unknown.

Recent progress in oxide film growth suggests that the defect type, ordering, and density can be controlled by a proper choice of deposition conditions.^[13] In addition, model systems such as bicrystal grain boundaries allow atomically defined defects to be created. Below, we summarize some recent advances in probing the atomic and electronic structure of defects, their effects on ferroelectric polarization, and polarization switching mechanisms on a single-defect level.

2. Atomic and Electronic Structure and Order Parameter Imaging at Defects

Ferroelectrics are complex materials with a hierarchy of characteristic structural length scales, from domains hundreds of nanometers in size to intra-unit cell ionic displacements of fractions of an angstrom. In this section we give a brief overview of what information can be obtained from transmission electron microscopy (TEM) studies on each of the relevant length scales, as well as an outlook towards dynamic studies.

Observations without lattice resolution, on length scales from several micrometers to several nanometers, characterize the mesoscopic domain structure and the nature of defects such as dislocations and grain boundaries. Ferroelectric domain structures were among the earliest observations of lattice defects by TEM. Since Hirsch et al.^[14] formulated the kinematical theory of diffraction contrast, it became possible to establish the optimal observation conditions for dislocations, stacking faults, and other defects, as well as to quantitatively determine geometric parameters such as Burgers vectors. Observations of ferroelectric domain structures immediately followed, starting with 90° and 180° (Fig. 2a) domain walls in BTO^[15] and progressing to more complex structures.

On a finer length scale, from a few nanometers to several angstroms (unit-cell scale), misfit dislocations and dislocation arrays in ferroelectric thin films can be visualized (Fig. 2b, c).^[13] With high-resolution (HR) TEM, Burgers vectors can be determined directly from an image (Fig. 2d) by counting atomic planes. When domain walls are associated with lattice strain, such as a 90° domain wall in BTO, they can also be visualized directly, and their relation to interface dislocations can be examined (Fig. 2e, f).^[12]

On the atomic scale – 1 to 2 angstroms or even subangstrom – the instrumental component becomes critical. The universal tendency in microscopy research is the drive for ever higher resolution but for a long time TEM was limited in its performance to more than 50 times the electron wavelength due to spherical aberration (C_s). As aberration correction^[16,17] became reality over the past 10 years, it brought an unprecedented expansion in capabilities for the examination of ever finer structural features. While point resolution improved to subangstrom values,^[18] signal-to-noise parameters of the images also improved, enabling more accurate detection and even quantification of the light elements from images, thus bringing refinement to defect studies. For example, Jia and Urban^[19] investigated twin boundaries in BTO (Fig. 2g) using negative C_s imaging and, in conjunction with image simulations, were able to determine the detailed structure of the boundary, including reduced oxygen occupancy in some interfacial atomic columns.

Another advantage of aberration-corrected imaging is the ability to determine atomic positions with the accuracy of a few picometers. This has enabled a veritable breakthrough in ferroelectric characterization, bringing the capability to examine the

polarization and valence states on a single-unit-cell level. Jia et al.^[20] used HRTEM to directly image ferroelectric displacements in Pb(Zr,Ti)O₃ (PZT) thin films (Fig. 2h–j). The transition from non-ferroelectric SrRuO₃ (SRO) to PZT and the polarization

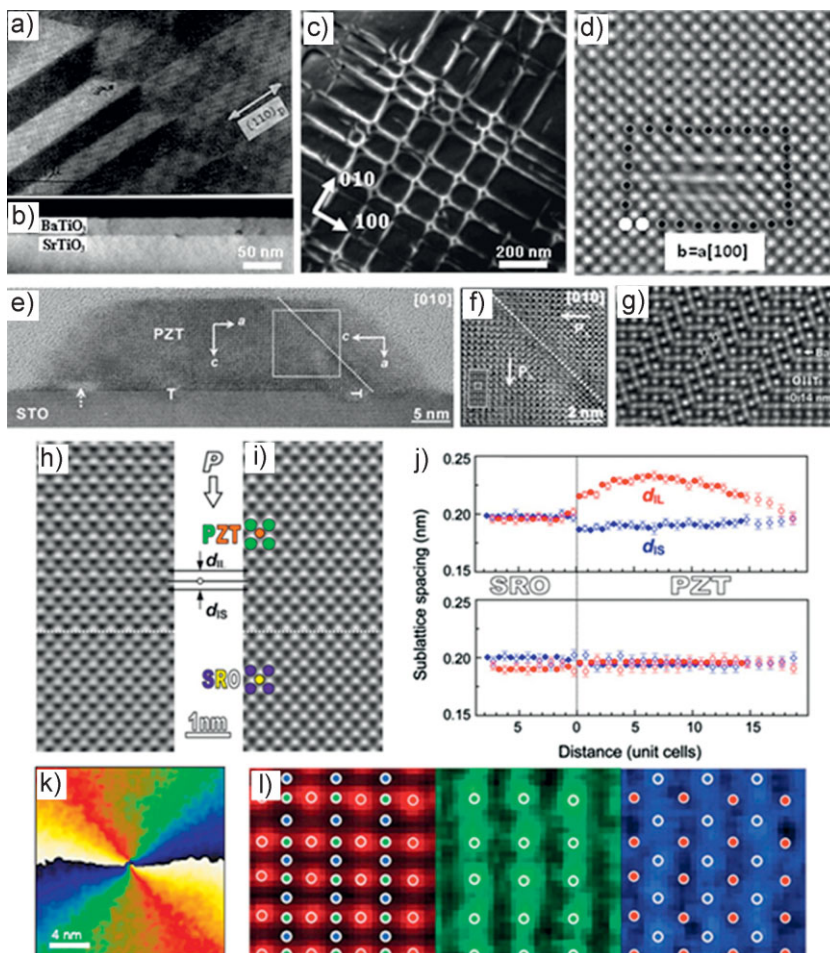


Figure 2. a) *a-c* domain structure in BTO. b) Cross-sectional dark-field image of a 20-nm BTO/STO film showing the dislocation cores at the interface. c) Plan-view dark-field image of the same BTO/STO film displaying a dislocation array. d) HRTEM image of a dislocation core at the film/substrate interface. e) Cross-sectional HRTEM image of a PZT island viewed along the (010) zone axis; dashed arrow represents a partial dislocation, T marks edge dislocations, dashed line marks a 90° twin wall. The region in the square is shown magnified in (f), the dashed line marking a 90° twin wall and P_s marks the vector of spontaneous polarization along the *c* axis. g) Magnified image of the twinned area of the BaTiO₃. The two vertical dark arrows indicate, as an example, two of the oxygen-atom positions in the twin-boundary plane. h) Average lattice image of the ferroelectric film. i) The calculated image, with the polarization direction of the PZT film shown by the arrow *P*, pointing from the film interior to the interface of PZT/SRO. White dotted lines mark the SRO/PZT interface. The cation positions are indicated by circles, Pb in green, Zr/Ti in red, Sr in violet, and Ru in yellow. j) Off-center cation displacements (resulting in polarization) across the SRO/PZT interface both normal to the interface (top) and along the interface (bottom). k) Experimentally measured radial displacement field around a screw dislocation in Si. l) HAADF image (red) and a set of two elemental maps obtained from an EELS image of STO, Ti in green and O in blue; atomic resolution is evident in all maps. Panel (a) reprinted with permission from [15]. Copyright 1964, Institute of Pure and Applied Physics of Japan. Panels (b–d) reprinted with permission from [13]. Copyright 2004, American Institute of Physics. Panels (e) and (f) reprinted with permission from [23]. Copyright 2005, American Physical Society. Panel (g) reprinted with permission from [19]. Copyright 2004, American Association for the Advancement of Science. Panels (h–j) and (k) reprinted with permission from [20] and [21]. Copyright 2007 and 2003, respectively, Nature Publishing Group. Panel (l) reprinted from [29]. Copyright 2009, Oxford University press.

change across a domain wall could be visualized, providing a direct measure of domain-wall and interface widths. For the first time, truly atomic-scale characterization of ferroelectricity becomes possible.

Several remarkable advances in the general field of electron microscopy have yet to be used for studies of defects in ferroelectric materials and are likely to produce interesting results in the field in the near future. For example, mapping of the strain-related atomic displacements via HRTEM and geometric-phase analysis can have direct relevance to such studies. Hytch et al.^[21] used this technique to map the displacement field associated with a dislocation in Si (Fig. 2k); the resulting strain map differed from the theoretically calculated displacement field by no more than 0.03 Å in any point of the image.

Another field that will undoubtedly produce new insight into structure and properties of ferroelectrics is scanning transmission electron microscopy (STEM), specifically high-angle annular dark-field (HAADF) imaging. Atomic column intensity in HAADF STEM imaging depends on the atomic number ($\approx Z^2$), which provides chemical identification of columns and is responsible for the alternative name for the technique, which is Z-contrast STEM.^[22] This technique was utilized for a number of defect-structure determinations,^[23] in particular, core structures of dislocations in the bulk and at grain boundaries in perovskites.^[24] However, the real power of the STEM setup lies in the ability to simultaneously acquire electron energy loss spectra (EELS). Characteristic spectral features can be used to quantify the composition and to trace valence and electronic structure changes with atomic-column resolution. For example, STEM/EELS studies of 36° grain boundaries in SrTiO₃ (STO) demonstrated that dislocation cores at pristine grain boundaries have net positive charge due to incomplete TiO_x octahedra, which is alleviated on Mn doping via Mn³⁺/Ti⁴⁺ substitution at the core.^[25] Thus, accurate structure determination can help determine the charge of the dislocation core and the atomic-scale electrical properties of the grain boundary, opening the possibilities for studies of ferroelectric breakdown and fatigue and possibly of “dead layers”. With the latest generation of aberration-corrected STEMs, recording EELS scans on a two-dimensional (2D) array of points becomes feasible, producing atomic-resolution spectroscopic images for different elemental sublattices (Fig. 2l).^[26–29] Size and shape of the features in these images for different energy ranges are affected by composition, structure, and physical properties of the samples as well as by electron scattering inside the crystal. 2D information allows for better comparison with theory, which is necessary to distinguish these separate contributions.

It is therefore clear that in their static configuration ferroelectrics and associated defects can be comprehensively characterized by (S)TEM on a variety of length scales. However, dynamic studies are only performed below lattice resolution. All of these studies to date, including the most recent ones by the Tan group,^[30] investigated switching dynamics of ferroelectric single crystals and ceramics by applying a macroscopic electric field inside the electron microscope using specially designed sample holders. The observation of domain structure evolution with increasing field and its return almost to the original form at zero field in BTO single crystals suggests that the domain walls are pinned by internal defects. Switching-induced fracture was

also reported in most of the systems studied. However, very limited quantitative information can be extracted from the bulk-biasing setup, since there is no control over where the new domains are formed or how the domain walls move. In contrast, some novel approaches, such as specimen holders incorporating scanning tunneling microscopy (STM) tips,^[31] can enable local switching studies using field confinement by a biased scanning probe microscopy (SPM) probe.

3. Probing Local Polarization Switching Mechanisms in Ferroelectric Materials

The emergence of SPM-based techniques has allowed the functionality of materials to be probed at the nanometer level. A spectacular example is molecular-unfolding spectroscopy, which has opened a pathway for probing kinetics and thermodynamics of macromolecular reactions on a single-molecule level. Combined with advances in genetic engineering, this allows systematic studies of weak interactions and emergent behavior in biological macromolecules – the very foundations of life. This progress is enabled by the inherently quantitative nature of this technique, that is, the response is probed on a single molecule. In comparison, most SPM techniques on surfaces determine the response from multiple structural elements and are strongly limited by uncertainty in the signal generation volume (e.g., are controlled by the tip–surface contact area and surface and tip roughness). Below, we briefly discuss the operating principles of piezoresponse force microscopy (PFM) and its applicability to studying bias-induced phase transitions in solids.

3.1. Piezoresponse Force Microscopy and Spectroscopy

The detection mechanism in PFM is underpinned by the strong coupling between polarization and electromechanical response in ferroelectric materials. Combined with the ability of atomic force microscopy (AFM) to precisely measure small (≈ 10 pm) vertical displacements with nanometer lateral resolution, this allows static and dynamic polarization to be probed on the nanometer scale.

In PFM, a local electric field is generated by applying an AC voltage to a conducting AFM tip. This alternating field causes the ferroelectric material beneath the tip to deform (expand and contract with the field). The deformation is then detected as a tip deflection at the modulation voltage using the AFM electronics. The magnitude of the deflection is directly related to the piezoelectric coefficient of the probed material, which, in the case of ferroelectrics, is coupled to the polarization. The unique aspect of PFM is that the measured signal is independent (for good electrical tip–surface contact) of the contact radius and, hence, is only weakly sensitive to surface topography (Fig. 3a, b). This is in contrast to, for example, AFM-based elasticity and adhesion measurements, in which the stiffness of the tip–contact junction scales linearly with the contact radius. This weak sensitivity to topographic crosstalk renders PFM measurements quantitative; however, special attention has to be paid to the sample surface state during the sample preparation process. PFM can be used to map ferroelectric domains in a variety of systems over a range of

length scales from tens of micrometers to tens of nanometers (Fig. 3c) and below.

This approach can be directly extended to probe local polarization dynamics. The probe concentrates an electric field to a nanoscale volume of material approximately 10 nm in diameter (Fig. 3d), and induces local domain formation. Simultaneously, the probe detects the onset of nucleation and the size of a forming domain via detection of the electro-mechanical response of the material to a small AC bias^[32] or direct detection of strain.^[10] The local hysteresis loops thus obtained contain information on the domain nucleation and growth processes. In switching spectroscopy PFM (SS-PFM), the hysteresis loops are acquired at each point of the image and analyzed to yield 2D maps of coercive and nucleation biases, imprint, work of switching, and switchable polarization.

3.2. Mapping Polarization Statics and Dynamics by PFM and SS-PFM

The capability to manipulate polarization states in ferroelectric materials using a biased PFM tip has attracted much attention, both as the basis of ferroelectric data storage and as a pathway to study the physics of ferroelectric materials. Two approaches for mapping polarization dynamics in ferroelectrics have emerged. In capacitor-based experiments, the electric field is uniform across the device structure, and the PFM tip is used as a detector of local strain. This approach was extensively developed by, among others, the groups of Gruverman, Stolichnov, and Noh, and allows for mapping of the nucleation and domain growth in ferroelectric structures.^[33–35] A continuous high-speed imaging PFM as developed by the Huey group is an example of a similar approach.^[36] In capacitor experiments, polarization dynamics are determined by the interplay between nucleation at pre-existing domain sites and domain-wall motion.

Recently, SS-PFM using a tip electrode has allowed polarization switching to be studied at a pre-selected region on a surface. The variation of nucleation bias along the surface has been used to map the random-field (RF) and random-bond (RB) components of the disorder potential (Fig. 3e).^[37] In many cases, hysteresis loops in the vicinity of defects were found to possess intricate fine structure formed by the interaction of nascent domains with the strain fields of the defect. Recently, it has been demonstrated that the effect of a *single* (unidentified) localized defect on the thermodynamics of local polarization switching can be determined (Fig. 3f–i).^[38] However, elucidation of relevant mesoscopic and atomistic mechanisms requires a) appropriate

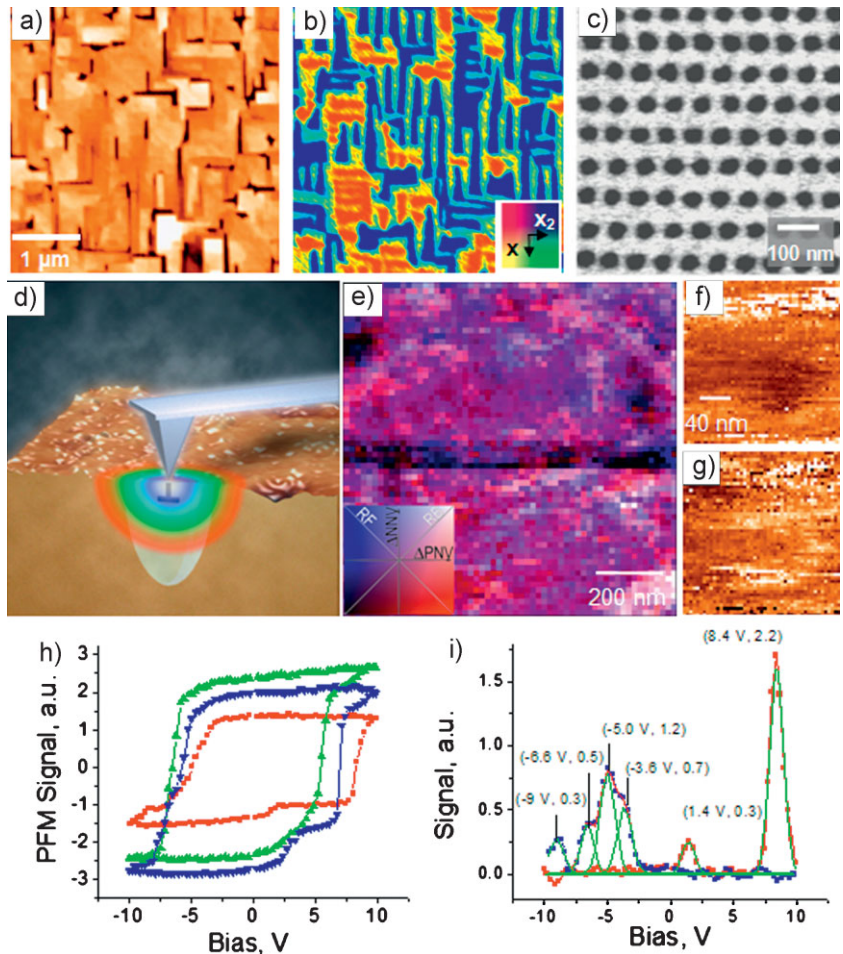


Figure 3. a) Topography [50] and b) vector PFM images of a BiFeO₃(BFO)/La_{0.7}Sr_{0.3}MnO₃ film. c) PFM image of a large array of written domains in PZT. d) The confinement of an electric field by an AFM probe allows the bias-induced phase transition within a defect-free volume or at a given separation from defects to be probed. e) The color map illustrates the RF and RB disorder potential in an epitaxial PZT film, allowing visualization of defects that favor one polarization orientation (RF) and strain fields that can destabilize the ferroelectric phase (RB). f, g) A single defect in multiferroic BFO determined from the nucleation bias and fine structure features on a h, i) hysteresis loop. Panels (c) and (f–i) reprinted with permission from [51] and [38]. Copyright 2002 and 2008, respectively, American Physical Society. Panels (d) and (e) reprinted with permission from [52] and [37], respectively. Copyright 2008, Elsevier and Nature Publishing Group, respectively.

theoretical developments and b) knowledge of the mesoscopic and atomic structure of the defects involved.

3.3. Mesoscopic Mechanisms

The potential of SS-PFM to provide quantitative and reproducible measurements has necessitated development of a theoretical description of the nanoscale polarization-switching mechanism. Simple estimates based on activation energy, as well as recent first-principles calculations, suggest that the characteristic size of the critical nucleus in polarization switching is on the order of a few nanometers. At the same time, the electric field produced by a PFM probe is essentially uniform below a 10–20-nm level. Therefore, the polarization-switching mechanism in the localized

field of the tip and in a uniform field can be expected to be equivalent. At the same time, the characteristic spacing between extended defects in a high-quality epitaxial film can be of the order of $\approx 100\text{--}300$ nm. Hence, PFM allows polarization switching to be studied in the vicinity of a single defect and corresponding deterministic mesoscopic mechanisms can be identified.

A ferroelectric thin film, particularly during switching, is rarely uniform, that is, it almost always contains rather complex domain structures with inhomogeneous polarization/electric field and strain/stress fields. A powerful approach to predicting domain structures and domain switching is the phase-field method, in which a domain structure is described by the spatial distributions of the local polarization.^[39] Thermodynamics are modeled by a Ginzburg–Landau free-energy functional that includes the bulk chemical free-energy density and the polarization gradient energy. The spatial distribution of polarization is then evolved by solving the time-dependent Ginzburg–Landau equations coupled with elasticity and electrostatic solutions for an inhomogeneous domain structure

$$\frac{\partial P_i(\mathbf{x}, t)}{\partial t} = -M \frac{\delta F}{\delta P_i(\mathbf{x}, t)} \quad (1)$$

where M is a kinetic coefficient related to the domain mobility, $\mathbf{x} = (x_1, x_2, x_3)$, t are the spatial and time coordinates, respectively, and $i = 1, 2, 3$. The spontaneous polarization $P = (P_1, P_2, P_3)$ is chosen as the order parameter. The total free energy F includes the bulk free energy F_{bulk} , domain-wall energy F_{wall} , elastic energy F_{elas} , and electrostatic energy F_{elec} , that is, $F_{\text{bulk}} + F_{\text{wall}} + F_{\text{elas}} + F_{\text{elec}}$.

Mechanically, the top surface is stress free and the bottom surface is constrained by a substrate. For modeling either uniform or local switching, the electrostatic boundary conditions are specified by the electrostatic potential distributions on the top and bottom surfaces of a film. For example, to model the applied electric field by a PFM tip, the electrostatic potentials can be specified as,

$$\phi_{\text{substrate-film interface}} = 0, \phi_{\text{film surface}} = \phi_1(x_1, x_2) \quad (2)$$

where ϕ_1 is assumed to have a 2D Lorentz-like distribution

$$\phi_1(x_1, x_2) = \phi_0 \left[\frac{\gamma^2}{(x_1 - x_1^{\text{tip}})^2 + (x_2 - x_2^{\text{tip}})^2 + \gamma^2} \right] \quad (3)$$

where $(x_1^{\text{tip}}, x_2^{\text{tip}})$ is the location of the tip (the peak of the distribution), and γ is the scale parameter that specifies the half-width at half-maximum.

It is possible to introduce structural defects such as dislocations using the micromechanics concept of eigenstrains or electrical defects by specifying the charge-density distribution. Similarly, structural defects such as grain boundaries can be modeled by introducing additional fields to specify the orientations of grains.

The fundamental aspect of polarization switching in this phase-field model is that the switching is intrinsic, and no thermal fluctuations or (unknown) defects are involved in the process. The comparison of phase-field modeling and SS-PFM

results of a defect-free surface has demonstrated that experimentally measured nucleation biases are well within a factor of two from theoretical phase-field predictions.^[40] In comparison, in capacitor structures the nucleation voltage is 2–3 orders of magnitude below the thermodynamic limit.

The understanding of polarization switching mechanisms on a defect-free surface suggests that a similar methodology can be used to determine how the presence of a defect affects switching. Recently, the in-plane a domains and $a_1\text{--}a_2$ domain junctions in tetragonal (100) ferroelectrics were shown to be the preferential nucleation sites for polarization switching, and the underlying mesoscopic mechanisms were determined. In rhombohedral ferroelectrics, the in-plane ferroelastic domain wall was shown to control the kinetics of ferroelectric switching and, hence, device behavior. Finally, polarization switching on a well-defined bicrystal grain boundary has been studied, and the origin of the observed behavior has been traced to the formation of an unusual ferroelectric–ferroelastic nucleus.^[41]

4. Future Challenges and Opportunities

The understanding and control of polarization-switching mechanisms at the level of a single defect offers breakthroughs in physics and materials science, as well as new applications ranging from low-voltage high-endurance non-volatile memories to near-atomic-level storage, and to new classes of devices utilizing polarization to underpin functionality. Progress in these applications requires the identification of the atomic mechanism, necessitating the solution of the twofold problem of instrumental development and quantitative data analysis.

4.1. Techniques

Much of the progress in the understanding of nanoscale ferroelectrics has been precipitated by the development of PFM and associated spectroscopic techniques. At the same time, the potential for future advances is extraordinarily large. The use of resonance enhancement in PFM through the band excitation^[42] and dual-frequency^[43] resonance tracking (once data analysis and interpretation problems are resolved) and compound cantilevers^[44] will allow measurements of weakly piezoelectric materials, as well as a $\sim 10\text{--}100$ -fold increase in energy resolution, signal-to-noise ratio, and reduction in image acquisition times in SS-PFM.

A significant impact can be achieved in combining PFM with other local probe techniques that provide additional information on material properties, including near-field optical and microwave microscopy and Raman spectroscopy. This will allow changes in local chemical composition to be mapped, polarization-switching mechanisms to be distinguished, and ultrafast phenomena to be located. This unique opportunity is offered by the combination of voltage spectroscopy and scanning non-linear dielectric microscopy, introduced and perfected by the Cho group.^[7] The combination of these techniques offers the potential for measurements to be taken with 1–3-nm spatial resolution,

which is beginning to approach the level of the single perovskite unit cell.

Unique potential for studying atomistic mechanisms of polarization switching and the interaction between polarization, strains, and electronic effects is offered by combining local electrical excitation by the SPM probe with high-resolution structural and electronic structure imaging with high-resolution electron microscopy and focused X-ray microscopy (Fig. 4). While these techniques impose a number of restrictions on sample geometry (the need for a thin TEM sample, for example) or still have not achieved sufficient sensitivity, this is clearly something that is likely to be achieved in the near future. In these methods, PFM will allow control of the location of the electric field inside the material, and STEM or X-ray microscopy will allow mapping of the switching mechanisms and resulting changes in material structure. Finally, these advances will require control of the surface chemistry of the material, necessary to control depolarization behavior, which can be achieved through in situ growth.

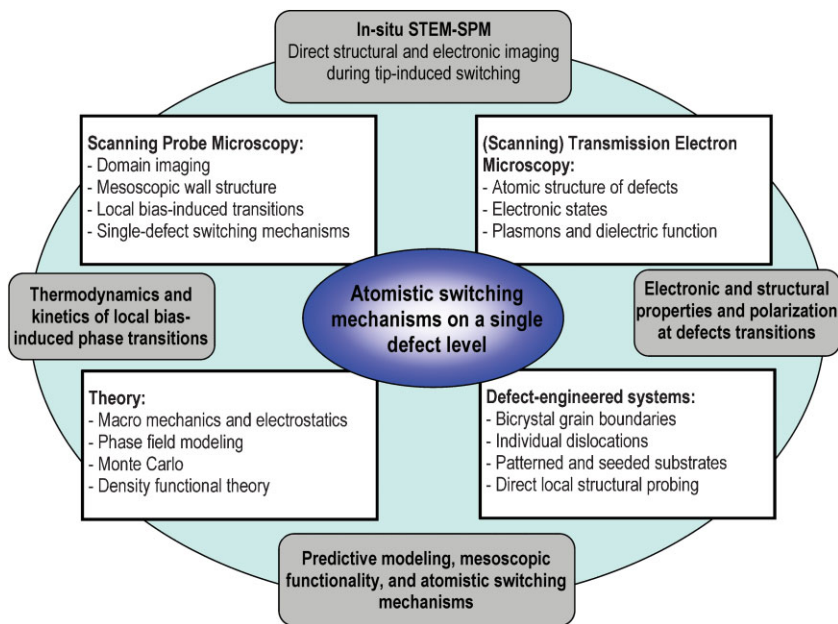


Figure 4. The synergy between scanning probe and electron microscopy, theory, and defect-engineered systems required to decipher atomistic polarization switching mechanisms at a single-defect level.

4.2. Multidimensional Data Analysis

The development of SS-PFM and similar spectroscopic techniques as well as combined techniques, such as voltage spectroscopy and scanning non-linear dielectric microscopy, allows probing of the spatial variability of switching behavior across the surface. However, in SS-PFM the relevant information is distributed across a full 3D data set, rather than concentrated in a single spectroscopy curve. For single-point measurements on a nearly ideal surface or for a known defect location, an extensive analytical framework has been developed for the analysis of bias-induced phase transitions from a single spectrum:

1. Describe the thermodynamics of bias-induced switching including defect effects;
2. Determine the domain geometry for a given bias from the minimum of free energy;
3. Determine the signal as a convolution of domain and signal generation volume;
4. Calibrate the probe geometry.

The analytical solutions for this problem are scarce, and are unavailable for multidimensional data sets. The 3- and 4D spatially resolved spectroscopic tools necessitate data analysis in higher-dimensional parameter space, for example, manifested as correlations between spectra in adjacent locations, which are generally beyond our ability to visualize and comprehend. Correlative models based on artificial neural networks^[45] may offer a solution, wherein phase-field modeling or density functional theory is used to generate high-dimensional spectroscopic-imaging data describing defects of various kinds for a range of tip parameters to predict experimental 3D sets.

The synergistic development of growth and characterization methods, theoretical models, and tools for theory–experiment comparison will allow polarization-switching mechanisms to be understood on the level of a single atomically defined defect, linking atomistic and mesoscopic scales. This will lead to a new understanding of bias-induced phase transitions in electrochemical systems, capacitors, phase-change memories, and a plethora of other systems. From this understanding will emerge the ability to control these processes, opening new pathways for device and energy applications.

Acknowledgements

The research was supported by the Divisions of Scientific User Facilities and Materials Sciences and Engineering, Office of Basic Energy Sciences, U.S. Department of Energy, by the ORNL Laboratory Directed research and Development Program and by appointment to the ORNL Postdoctoral Research Program administered jointly by ORNL and ORISE. BJR also acknowledges the support of UCD Research.

Received: March 7, 2009

Revised: May 22, 2009

Published online: July 27, 2009

- [1] National Nanotechnology Initiative 2006, <http://www.nano.gov/>.
- [2] M. E. Lines, A. M. Glass, *Principles and Applications of ferroelectrics and related Materials*, Oxford University Press, Oxford, UK 2001.
- [3] V. K. Wadhawan, *Introduction to Ferromagnetic Materials*, Gordon and Breach, Amsterdam 2000.

- [4] a) R. E. Reed-Hill, *Physical Metallurgy Principles*, PWS-Kent 3rd ed. CL-Engineering, Boston **1991**. b) F. R. N. Nabarro, *Philos. Mag. A* **1997**, *75*, 703.
- [5] J. Scott, in: *Ferroelectric Memories* (Eds: K. Itoh, T. Sakurai), Springer, Berlin **2000**.
- [6] T. Tybell, C. H. Ahn, J. M. Triscone, *Appl. Phys. Lett.* **1998**, *72*, 1454.
- [7] K. Tanaka, Y. Kurihashi, T. Uda, Y. Daimon, N. Odagawa, R. Hirose, Y. Hiranaga, Y. Cho, *Jpn. J. Appl. Phys.* **2008**, *47*, 3311.
- [8] J. Rodriguez Contreras, H. Kohlstedt, U. Poppe, R. Waser, C. Buchal, N. A. Pertsev, *Appl. Phys. Lett.* **2003**, *83*, 4595.
- [9] S. Ducharme, V. M. Fridkin, A. Bune, L. M. Blinov, S. P. Palto, S. G. Yudin, *Phys. Rev. Lett.* **2000**, *84*, 175.
- [10] P. Maksymovych, S. Jesse, P. Yu, R. Ramesh, A. P. Baddorf, S. V. Kalinin, *Science* **2009**, *324*, 1421.
- [11] A. Yu, Emelyanov, N. A. Pertsev, *Phys. Rev. B* **2003**, *68*, 214103.
- [12] M. W. Chu, I. Szafraniak, D. Hesse, M. Alexe, U. Gosele, *Phys. Rev. B* **2005**, *72*, 174112.
- [13] H. P. Sun, W. Tian, X. Q. Pan, J. H. Haeni, D. G. Schlom, *Appl. Phys. Lett.* **2004**, *84*, 3298.
- [14] P. B. Hirsch, A. Howie, M. J. Whelan, *Philos. Trans. R. Soc. A* **1960**, *252*, 499.
- [15] M. Tanaka, G. Honjo, *J. Phys. Soc. Jpn.* **1964**, *19*, 954.
- [16] O. L. Krivanek, N. Dellby, A. R. Lupini, *Ultramicroscopy* **1999**, *78*, 1.
- [17] M. Haider, H. Rose, S. Uhlemann, E. Schwan, B. Kabius, K. Urban, *Ultramicroscopy* **1998**, *75*, 53.
- [18] P. D. Nellist, M. F. Chisholm, N. Dellby, O. L. Krivanek, M. F. Murfitt, Z. S. Szilagyi, A. R. Lupini, A. Borisevich, W. H. Sides, S. J. Pennycook, *Science* **2004**, *305*, 1741.
- [19] C. L. Jia, K. Urban, *Science* **2004**, *303*, 2001.
- [20] C. L. Jia, V. Nagarajan, J.-Q. He, L. Houben, T. Zhao, R. Ramesh, K. Urban, R. Waser, *Nat. Mater.* **2007**, *6*, 64.
- [21] M. J. Hytch, J.-L. Putaux, J.-M. Penisson, *Nature* **2003**, *423*, 270.
- [22] S. J. Pennycook, D. E. Jesson, *Phys. Rev. Lett.* **1990**, *64*, 938.
- [23] M. M. McGibbon, N. D. Browning, M. F. Chisholm, *Science* **1994**, *266*, 102.
- [24] M. F. Chisholm, S. J. Pennycook, *Philos. Mag.* **2006**, *86*, 4699.
- [25] N. D. Browning, J. P. Buban, H. O. Moltaji, S. J. Pennycook, G. Duscher, K. D. Johnson, R. P. Rodrigues, V. P. Dravid, *Appl. Phys. Lett.* **1999**, *74*, 2638.
- [26] M. Bosman, M. Watanabe, D. T. L. Alexander, V. J. Keast, *Ultramicroscopy* **2006**, *106*, 1024.
- [27] K. Kimoto, T. Asaka, T. Nagai, M. Saito, Y. Matsui, K. Ishizuka, *Nature* **2007**, *450*, 702.
- [28] D. A. Muller, L. F. Kourkoutis, M. Murfitt, J. H. Song, H. Y. Hwang, J. Silcox, N. Dellby, O. L. Krivanek, *Science* **2008**, *319*, 1073.
- [29] S. J. Pennycook, M. Varela, A. R. Lupini, M. P. Oxley, M. F. Chisholm, *J. Electron Microsc.* **2009**, *58*, 87.
- [30] X. Tan, H. He, J.-K. Shang, *J. Mater. Res.* **2005**, *20*, 1641.
- [31] J. Cumings, E. Olsson, A. K. Petford-Long, Y. Zhu, *MRS Bull* **2008**, *33*, 101.
- [32] S. Jesse, H. N. Lee, S. V. Kalinin, *Rev. Sci. Instr.* **2006**, *77*, 073702.
- [33] A. Gruverman, B. J. Rodriguez, C. Dehoff, A. I. Kingon, R. J. Nemanich, *Appl. Phys. Lett.* **2005**, *87*, 082902.
- [34] I. Stolichnov, A. Tagantsev, N. Setter, J. S. Cross, M. Tsukada, *Appl. Phys. Lett.* **1999**, *74*, 3552.
- [35] D. J. Kim, J. Y. Jo, T. H. Kim, S. M. Yang, B. Chen, Y. S. Kim, T. W. Noh, *Appl. Phys. Lett.* **2007**, *91*, 132903.
- [36] R. Nath, Y.-H. Chu, N. A. Polomoff, R. Ramesh, B. D. Huey, *Appl. Phys. Lett.* **2008**, *93*, 072905.
- [37] S. Jesse, B. J. Rodriguez, S. Choudhury, A. P. Baddorf, I. Vrejoiu, D. Hesse, M. Alexe, E. A. Eliseev, A. N. Morozovska, J. Zhang, L. Q. Chen, S. V. Kalinin, *Nature Materials* **2008**, *7*, 209.
- [38] S. V. Kalinin, S. Jesse, B. J. Rodriguez, Y. H. Chu, R. Ramesh, E. A. Eliseev, A. N. Morozovska, *Phys. Rev. Lett.* **2008**, *100*, 155703.
- [39] L. Q. Chen, *J. Am. Ceram. Soc.* **2008**, *91*, 1835.
- [40] S. V. Kalinin, B. J. Rodriguez, S. Jesse, Y. H. Chu, T. Zhao, R. Ramesh, E. A. Eliseev, A. N. Morozovska, *Proc. Natl. Acad. Sci. USA* **2007**, *104*, 20204.
- [41] B. J. Rodriguez, S. Choudhury, Y. H. Chu, A. Bhattacharyya, S. Jesse, K. Seal, A. P. Baddorf, R. Ramesh, L.-Q. Chen, S. V. Kalinin, *Adv. Funct. Mater.* **2009**, *19*, 1.
- [42] S. Jesse, S. V. Kalinin, R. Proksch, A. P. Baddorf, B. J. Rodriguez, *Nanotechnology* **2007**, *18*, 435503.
- [43] B. J. Rodriguez, C. Callahan, S. V. Kalinin, R. Proksch, *Nanotechnology* **2007**, *18*, 475504.
- [44] B. Zeyen, K. Virwani, B. Pittenger, K. L. Turner, *Appl. Phys. Lett.* **2009**, *94*, 103507.
- [45] S. Haykin, *Neural Networks: A Comprehensive Foundation*, 2nd ed, Prentice Hall, Upper Saddle River, NJ **1998**.
- [46] C. H. Ahn, K. M. Rabe, J.-M. Triscone, *Science* **2004**, *303*, 488.
- [47] E. Y. Tsybal, H. Kohlstedt, *Science* **2006**, *313*, 181.
- [48] S. R. Summerfelt, T. S. Moise, G. Xing, L. Colombo, T. Sakoda, S. R. Gilbert, A. L. S. Loke, S. Ma, L. A. Wills, R. Kavari, T. Hsu, J. Armano, S. T. Johnson, D. J. Vestcyk, M. W. Russell, S. M. Bilodeau, P. van Buskirk, *Appl. Phys. Lett.* **2001**, *79*, 4004.
- [49] S. V. Kalinin, B. J. Rodriguez, S. Jesse, E. Karapetian, E. A. Eliseev, A. N. Morozovska, *Annu. Rev. Mat. Res.* **2007**, *37*, 189.
- [50] N. Balke, S. Choudhury, S. Jesse, M. Huijben, Y.H. Chu, A.P. Baddorf, L.Q. Chen, R. Ramesh, S.V. Kalinin, unpublished.
- [51] T. Tybell, P. Paruch, T. Giamarchi, J.-M. Triscone, *Phys. Rev. Lett.* **2002**, *89*, 097601.
- [52] S. V. Kalinin, B. J. Rodriguez, S. Jesse, P. Maksymovych, K. Seal, M. Nikiforov, A. P. Baddorf, A. L. Kholkin, R. Proksch, *Materials Today* **2008**, *11*, 16.